Article

Properties of a Mixed-Valence (Fe)(Fe) Square Cell for Utilization in the Quantum Cellular Automata Paradigm for Molecular Electronics

Jieying Jiao, Gary J. Long, Leila Rebbouh, Fernande Grandjean, Alicia M. Beatty, and Thomas P. Fehlner

J. Am. Chem. Soc., **2005**, 127 (50), 17819-17831• DOI: 10.1021/ja0550935 • Publication Date (Web): 24 November 2005

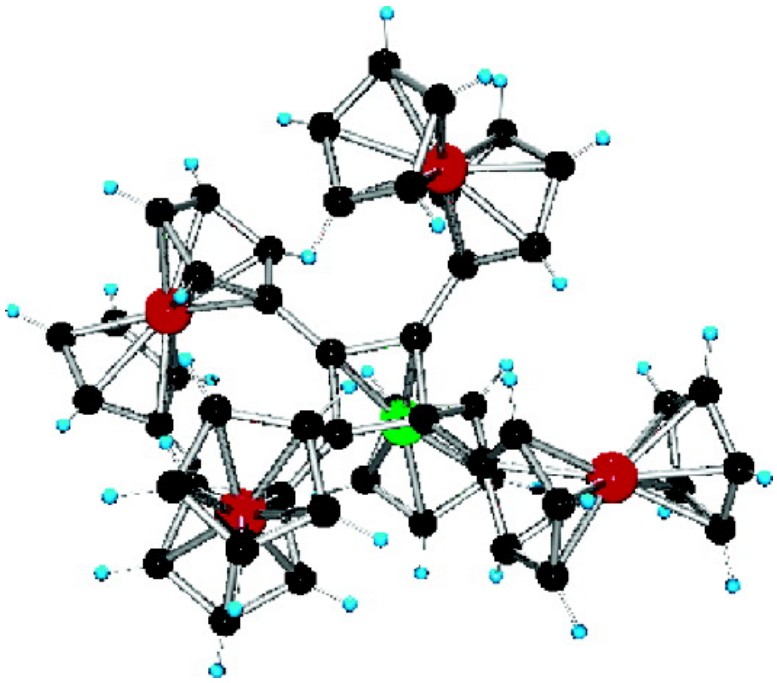

J|A|C|S
ARTICLES
Published on Web 11/24/2005

Properties of a Mixed-Valence $(Fe^{II})_2(Fe^{III})_2$ Square Cell for Utilization in the Quantum Cellular Automata Paradigm for Molecular Electronics

Jieying Jiao,[†] Gary J. Long,[‡] Leila Rebbouh,[§] Fernande Grandjean,[§] Alicia M. Beatty,[†] and Thomas P. Fehlner*[,†]

Contribution from the Department of Chemistry & Biochemistry, University of Notre Dame, Notre Dame, Indiana 46556-5670, Department of Chemistry, University of Missouri—Rolla, Rolla, Missouri 65409-0010, and Department of Physics, B5, University of Liège, B-4000 Sart-Tilman, Belgium

Received July 27, 2005; E-mail: fehlner.1@nd.edu

Abstract: The di-mixed-valence complex $[\{(\eta^5\text{-}C_5H_5)Fe(\eta^5\text{-}C_5H_4)\}_4(\eta^4\text{-}C_4)Co(\eta^5\text{-}C_5H_5)]^{2+}$, $\mathbf{1}^{2+}$, has been evaluated as a molecular four-dot cell for the quantum cellular automata paradigm for electronic devices. The cations $\mathbf{1}^{1+}$ and $\mathbf{1}^{2+}$ are prepared in good yield by selective chemical oxidation of $\mathbf{1}^{0}$ and are isolated as pure crystalline materials. The solid-state structures of $\mathbf{1}^{0}$ and $\mathbf{1}^{1+}$ and the midrange- and near-IR spectra of $\mathbf{1}^{0}$, $\mathbf{1}^{1+}$, $\mathbf{1}^{2+}$, and $\mathbf{1}^{3+}$ have been determined. Further, the variable-temperature EPR spectra of $\mathbf{1}^{1+}$ and $\mathbf{1}^{2+}$, magnetic susceptibility of $\mathbf{1}^{1+}$ and $\mathbf{1}^{2+}$, Mössbauer spectra of $\mathbf{1}^{0}$, $\mathbf{1}^{1+}$, and $\mathbf{1}^{2+}$, NMR spectra of $\mathbf{1}^{0}$, and paramagnetic NMR spectra of $\mathbf{1}^{1+}$ and $\mathbf{1}^{2+}$ have been measured. The X-ray structure determination reveals four ferrocene "dots" arranged in a square by C—C bonds to the corners of a cyclobutadiene linker. The four ferrocene units project from alternating sides of the cyclobutadiene ring and are twisted to minimize steric interactions both with the $Co(\eta^5\text{-}C_5H_5)$ fragment and with each other. In the solid state $\mathbf{1}^{2+}$ is a valence-trapped Robin and Day class II compound on the 10^{-12} s infrared time scale, the fastest technique used herein, and unambiguous evidence for two Fe^{II} and two Fe^{III} sites is observed in both the infrared and Mössbauer spectra. Both EPR and magnetic susceptibility measurements show no measurable spin—spin interaction in the solid state. In solution, the NMR spectra show that free rotation around the C—C bonds connecting the ferrocene units to the cyclobutadiene ring becomes increasingly hindered with decreasing temperature, leading to spectra at the lowest temperature that are consistent with the solid-state structure. Localization of the charges in the cations, which is observed in the paramagnetic NMR spectra as a function of temperature, correlates with the fluxional behavior. Hence, the alignment between the π systems of the central linker and the ferrocene moieties most likely controls the rate of electron exchange between the dots.

Introduction

The chemistry of mixed-valence complexes[1] joins that of molecular electronics[2,3] in the quantum cellular automata (QCA) paradigm.[4,5] In this novel approach to electronics, the binary language/current switch paradigm used so effectively in transistor-based devices is modified by replacing on/off current states by dipole orientation within a cell; i.e., current-driven switching of transistors is replaced by electric field coupling between adjacent dipolar cells, thereby correlating dipole orientations and transmitting binary instructions.[6] The QCA concept has been demonstrated theoretically as well as experimentally at low temperature to be a viable alternative to the present transistor-based technology.[7,8] However, for room-temperature operation the QCA paradigm requires the well-defined state energies of molecular-sized cells to generate energy differences between state configurations in the presence of a field larger than the thermal energy, kT, at practical temperatures.[9] In short QCA excels at the size scale where existing types of transistors must fail because of significant leakage currents and poor switching characteristics. Further, heat losses associated with QCA are orders of magnitude lower than those associated with devices based on current,[10] thereby giving molecular QCA an inherent capability of utilizing the device densities possible at molecular size scales without melting any feasible supporting substrate.

[†] University of Notre Dame.
[‡] University of Missouri—Rolla.
[§] University of Liège.

(1) Robin, M. B.; Day, P. *Adv. Inorg. Chem. Radiochem.* **1967**, *10*, 247—422.
(2) Aviram, A.; Ratner, M. A. *Chem. Phys. Lett.* **1974**, *29*, 277—283.
(3) Jortner, J.; Ratner, M. A. *Molecular Electronics*; Blackwell Science: Oxford, 1997.
(4) Lent, C. S.; Tougaw, P. D.; Porod, W.; Bernstein, G. H. *Nanotechnology* **1993**, *4*, 49—57.
(5) Tougaw, P. D.; Lent, C. S.; Porod, W. J. *J. Appl. Phys.* **1993**, *74*, 3558—3566.
(6) Lent, C. S. *Science* **2000**, *288*, 1597—1599.
(7) Orlov, A. O.; Amlani, I.; Bernstein, G. H.; Lent, C. S.; Snider, G. L. *Science* **1997**, *277*, 928—930.
(8) Amlani, I.; Orlov, A. O.; Toth, G.; Bernstein, G. H.; Lent, C. S.; Snider, G. L. *Science* **1999**, *284*, 289—291.
(9) Lent, C. S.; Isakaen, B.; Lieberman, M. *J. Am. Chem. Soc.* **2003**, *125*, 1056—1063.
(10) Timler, J.; Lent, C. S. *J. Appl. Phys.* **2002**, *91*, 823—831.

10.1021/ja0550935 CCC: $30.25

Scheme 1. Schematic Drawing of a Molecular Majority Gate Based on Five Tetranuclear Di-Mixed-Valence Complexes of Iron with Three Cells as Input, One as a Central Comparator, and One as the Output[a]

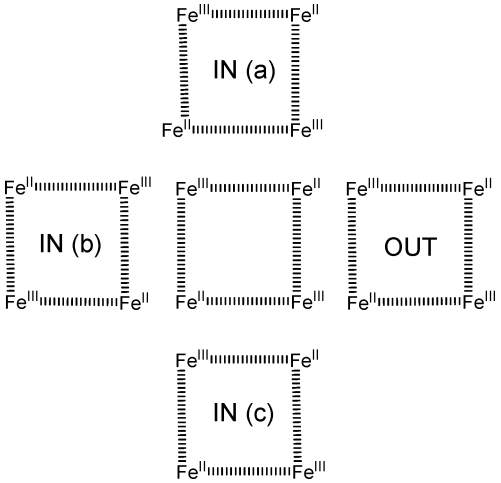

[a] Illustrated is one configuration of the truth table with inputs of (a) 1, (b) 0, and (c) 1 and an output of 1.

The simplest molecular QCA cell is a symmetric mixed-valence complex in which the binary states are represented by the location of a mobile electron at one metal center or the other. In molecular QCA individual cells must be coupled to, and switched by, the fields of adjacent cells. Although switching caused by absorption of photons of energy corresponding to the intervalence charge transfer band is well-known, only recently has controlled switching of surface-bound, oriented, mixed-valence complexes by an applied electric field been demonstrated.[11] The effects of unsymmetric and symmetric mixed-valence complexes, short- and long-chain alkyne linkers between metal centers, and counterion size on the switching potential have been subsequently investigated.[12] A logical next step is the development of a four-metal molecular QCA cell because such a molecule would be a more versatile building block for constructing logic units than a two-metal cell. Scheme 1 illustrates a simple majority gate that may be constructed from several four-dot cells or four-metal square molecules.[13]

Several successful strategies for rational syntheses of assemblies of metal complexes demonstrate the growing power of synthetic inorganic chemistry.[14−16] Four-metal systems are well represented, but it is the square array that meets one important criterion of molecular QCA; i.e., the di-mixed-valence state must be 2-fold degenerate. In other words, rectangular arrays are no better than dinuclear systems for QCA purposes, and tetrahedral arrays are completely useless. However, placing four metal centers in a symmetric, covalently bound square structure is only the first step leading to a four-metal QCA cell. The metal center used to build the square must have two stable, accessible oxidation states, and there must be sufficient interaction between these redox centers such that the four-metal complex in the di-mixed-valence state can be isolated as a pure compound without being labile with respect to charge disproportionation.

No such species has been isolated and characterized to date although there are a few reports of examples of square complexes that exhibit promising electrochemical behavior.[17−20] In addition to the potential application to molecular QCA, the nature of a di-mixed-valence state in a four-metal square has yet to be characterized. For example, the mixed-valence states of a triangular three-metal system have been investigated both experimentally and theoretically and reveal complications introduced by spin−spin interactions in the di-mixed-valence state.[21] Similar effects, if observed in a molecular square di-mixed-valence state, would complicate its intended application. Thus, in the following, a known molecular square is revisited and its synthetically accessible mixed-valence states have been characterized structurally and spectroscopically. Preliminary results have been communicated previously.[22]

Results and Discussion

The square array of tricobalt alkylidyne clusters supported by the quadruply bonded dimolybdenum central linker in $\{(CO)_9Co_3CCO_2\}_4Mo_2$ provides a good example of the problem faced herein.[23] The spectroscopic properties of this compound suggest significant electronic interaction between the linker and clusters,[23] and both the neutral and the radical anion of the tricobalt cluster are accessible.[24] However, an electrochemical investigation of the square cluster array shows a one-electron oxidation of the dimolydbenum core as expected but a single multielectron reduction of the cobalt clusters.[25] Effectively, the cobalt clusters act as independent reducible entities in the electrochemical experiment. Expressed in terms of chemical equilibrium, the comproportionation constants are too small to permit isolation of the direduced species.

The literature on dinuclear mixed-valence systems as well as additional work with the dimolybdenum carboxylate linker suggested a square with redox centers connected by alkyne linkers or the equivalent would be required.[19,26] A central cyclobutadiene linker and peripheral alkyne linkers between cis-octahedral corner units are two possibilities. We noted that a square of the first type, $\{(\eta^5\text{-}C_5H_5)Fe(\eta^5\text{-}C_5H_4)\}_4(\eta^4\text{-}C_4)Co(\eta^5\text{-}C_5H_5)$, **1^0**, with redox-active ferrocene centers had already been synthesized and spectroscopically characterized.[27] Despite the fact that the reported cyclic voltammetry seemed less than propitious for isolating the desired mixed-valence state with "a wave at 0.29 V with the remaining three redox waves blended

(11) Qi, H.; Sharma, S.; Li, Z.; Snider, G. L.; Orlov, A. O.; Lent, C. S.; Fehlner, T. P. *J. Am. Chem. Soc.* **2003**, *125*, 15250−15259.
(12) Qi, H.; Gupta, A.; Noll, B. C.; Snider, G. L.; Lu, Y.; Lent, C. S.; Fehlner, T. P. *J. Am. Chem. Soc.* **2005**, *127*, 15218−15227.
(13) Lent, C. S.; Tougaw, P. D. *J. Appl. Phys.* **1993**, *74*, 6227−6233.
(14) Leininger, S.; Olenyuk, B.; Stang, P. J. *Chem. Rev.* **2000**, *100*, 853−908.
(15) Holliday, B. J.; Mirkin, C. A. *Angew. Chem., Int. Ed.* **2001**, *40*, 2022−2043.
(16) Cotton, F. A.; Lin, C.; Murillo, C. A. *Acc. Chem. Res.* **2001**, *34*, 759−771.
(17) Cotton, F. A.; Lin, C.; Murillo, C. A. *J. Am. Chem. Soc.* **2001**, *123*, 2670−2671.
(18) Lau, V. C.; Berben, L. A.; Long, J. R. *J. Am. Chem. Soc.* **2002**, *124*, 9042−9043.
(19) Yao, H.; Sabat, M.; Grimes, R. N.; de Biani, F. F.; Zanello, P. *Angew. Chem., Int. Ed.* **2003**, *42*, 1002−1005.
(20) Kotz, J.; Neyhart, G.; Vining, W. J.; Rausch, M. D. *Organometallics* **1983**, *2*, 79−82.
(21) Weyland, T.; Costuas, K.; Toupet, L.; Halet, J.-F.; Lapinte, C. *Organometallics* **2000**, *19*, 4228−4239.
(22) Jiao, J. Y.; Long, G. J.; Grandjean, F.; Beatty, A. M.; Fehlner, T. P. *J. Am. Chem. Soc.* **2003**, *125*, 7522−7523.
(23) Cen, W.; Lindenfeld, P.; Fehlner, T. P. *J. Am. Chem. Soc.* **1992**, *114*, 5451−5452.
(24) Hinkelmann, K.; Heinze, J.; Schacht, H.-T.; Field, J. S.; Vahrenkamp, H. *J. Am. Chem. Soc.* **1989**, *111*, 5078−5091.
(25) Cen, W. Ph.D. Thesis, University of Notre Dame, Notre Dame, IN, 1992.
(26) Ward, M. D. *Chem. Soc. Rev.* **1995**, 121−134.
(27) Rausch, M. D.; Higbie, F. A.; Westover, G. F.; Clearfield, A.; Gopal, R.; Troup, J. M.; Bernal, I. *J. Organomet. Chem.* **1978**, *149*, 245−264.

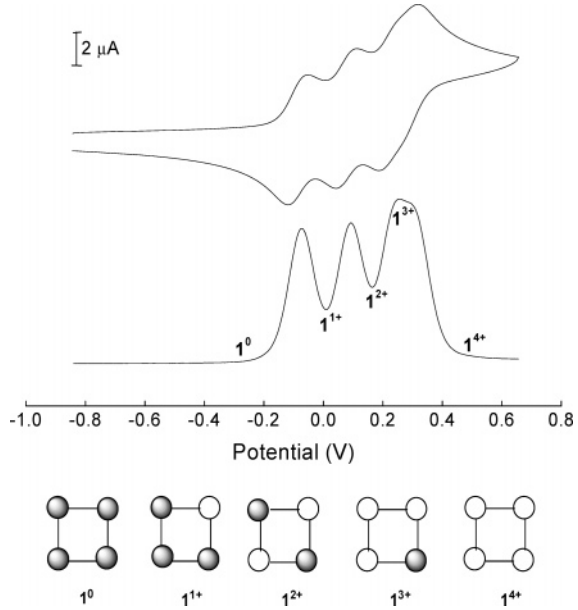

Figure 1. Cyclic and square wave voltammetry of $\{(\eta^5\text{-}C_5H_5)Fe(\eta^5\text{-}C_5H_4)\}_4(\eta^4\text{-}C_4)Co(\eta^5\text{-}C_5H_5)$, $\mathbf{1^0}$, at 100 mV s^{-1} in CH_2Cl_2/CH_3CN mixed solvent ($E_{1/2}$(ferrocenium/ferrocene) = 0.344 V). The five oxidation states (Fe^{II}, gray; Fe^{III}, white) are represented at the bottom of the figure, and the numbers on the square wave data indicate the potentials at which each is stable.

into a broad wave centered at ≈0.4 V",[20] reexamination of the compound was carried out because visible and near-IR bands had been reported for the 1+ through 3+ cations produced by bulk electrolysis. In addition, for our purposes we could think of no better square based on a central linker. As now described below, the desired mixed-valence compound could be isolated and characterized as a pure compound.

Synthesis of $\mathbf{1^0}$. Neutral $\mathbf{1^0}$ was synthesized from biferrocenylacetylene and $(\eta^5\text{-}C_5H_5)Co(CO)_2$ following the route reported in the original work.[27] The yield of analytically pure crystalline $\mathbf{1^0}$ from the alkyne dimerization reaction was 60%, and the spectroscopic data for the compound agreed with those in the literature.

Electrochemistry. The initial cyclic voltammetric experiments showed that both attention to the inert atmosphere and the choice of solvent were important. In the wrong solvents precipitation of oxidiation products on the electrode as the cationic charge increased caused complications in the cyclic voltammetric curves.[28] However, in a 1:1 mixture of CH_3CN and CH_2Cl_2 the cyclic and square wave voltammetry gave good resolution with unambiguous evidence of three redox couples (Figure 1). In addition, the unresolved structure in the peak at the most positive potential in the square wave voltammetry suggests the presence of a fourth couple. The $E_{1/2}$ potentials for the $\mathbf{1^0}/\mathbf{1^{1+}}$, $\mathbf{1^{1+}}/\mathbf{1^{2+}}$, $\mathbf{1^{2+}}/\mathbf{1^{3+}}$, and $\mathbf{1^{3+}}/\mathbf{1^{4+}}$ couples are −0.085, 0.075, 0.225, and 0.283 V, respectively ($\Delta E_p = 0.08 \pm 0.02$ V), relative to the potential for the ferrocene/ferrocenium couple. The potential differences between the redox waves are 160, 150, and 58 mV, from which the following comproportionation equilibria can be generated:

$$\mathbf{1^0} + \mathbf{1^{2+}} \rightleftarrows 2(\mathbf{1^{1+}}) \qquad K_{com} = 510$$

$$\mathbf{1^{1+}} + \mathbf{1^{3+}} \rightleftarrows 2(\mathbf{1^{2+}}) \qquad K_{com} = 346$$

$$\mathbf{1^{2+}} + \mathbf{1^{4+}} \rightleftarrows 2(\mathbf{1^{3+}}) \qquad K_{com} = 10$$

Hence, it appears likely that $\mathbf{1^{1+}}$, $\mathbf{1^{2+}}$, and $\mathbf{1^{4+}}$ could be isolated but not $\mathbf{1^{3+}}$.

Syntheses of the Cations. As the ferrocene/ferrocenium couple is 0.085 V more positive than the $\mathbf{1^0}/\mathbf{1^{1+}}$ couple and 0.075 V more negative than the $\mathbf{1^{1+}}/\mathbf{1^{2+}}$ couple, ferrocenium was the oxidizing agent of choice for the selective synthesis of $\mathbf{1^{1+}}$. It has the advantage that ferrocene could be easily removed from the cationic product. Addition of a stoichiometric amount of ferrocenium hexafluorophosphate to brown-orange $\mathbf{1^0}$ permitted the isolation of a 76% yield of deep brown $[\mathbf{1^{1+}}][PF_6]$ as an analytically pure crystalline solid. For the second oxidation a number of potentially suitable oxidants from the Connelly and Geiger review[29] were tested, and acetylferrocenium ion (formal potential of 0.27 V in CH_2Cl_2 and therefore a sufficiently powerful oxidizing agent to form the trication as well) was found satisfactory. Addition of 2 equiv to $\mathbf{1^0}$ gave a 95% yield of red-brown $[\mathbf{1^{2+}}][PF_6]_2$ as an analytically pure powder. As a check, it was demonstrated that $\mathbf{1^{1+}}$ could be cleanly converted into $\mathbf{1^{2+}}$ with 1 equiv of acetylferrocenium ion. For the IR work, the tetrafluoroborate salts were similarly prepared, and for the paramagnetic NMR study of $\mathbf{1^{2+}}$, the $[CF_3SO_3]^-$ salt was prepared.

Attempts were made to synthesize $\mathbf{1^{3+}}$ and $\mathbf{1^{4+}}$; however, in these cases pure materials could not be obtained. Treatment of $\mathbf{1^0}$ with excess acetylferrocenium ion gave a mixture which provided spectroscopic evidence of the presence of the trication (see below), but it could not be further purified. Changes in the spectroscopic data with time suggest that disproportionation into $\mathbf{1^{2+}}$ and $\mathbf{1^{4+}}$ does occur in accord with the electrochemical data. Likewise, treatment of $\mathbf{1^0}$ with 1,1′-diacetylferrocenium (formal potential of 0.49 V) produced a new solid product presumed to be $\mathbf{1^{4+}}$, but attempts to satisfactorily purify this low-solubility material were also unsuccessful.

Solid-State Structures. Crystals of $\mathbf{1^0}$ and $\mathbf{1^{1+}}$ suitable for a solid-state X-ray diffraction study were obtained by slow diffusion of hexane into CH_2Cl_2 solutions. All attempts to grow suitable single crystals of $\mathbf{1^{2+}}$ resulted in significant decomposition. The structures of $\mathbf{1^0}$ and $\mathbf{1^{1+}}$ obtained at 100 K are shown in Figures 2 and 3. Even though a counterion accompanies $\mathbf{1^{1+}}$ in the solid state, the ferrocene arrays are similar in both shape and dimensions. As the structure of neutral $\mathbf{1^0}$ is of higher quality, its structure is discussed first and the pertinent differences in the structures of $\mathbf{1^0}$ and $\mathbf{1^{1+}}$ are then noted.

The solid-state structure of $\mathbf{1^0}$ confirms the structure proposed originally on the basis of spectroscopic data[27] and provides structural metrics. The cyclobutadienyl ring is square, planar, and nearly parallel to the cyclopentadienyl ligand of the cobalt center. The bond distances from the rings to the central cobalt are normal. The ferrocenyl substituents of the cyclobutadienyl ring are twisted about the connecting C−C bonds with alternating torsion angles of −11° and 60°. Consequently, as shown in the side view in Figure 2, the Fe centers lie above and below

(28) Bard, A. J.; Faulkner, L. R. *Electrochemical Methods*; Wiley: New York, 2001.

(29) Connelly, N. G.; Geiger, W. E. *Chem. Rev.* **1996**, *96*, 877−910.

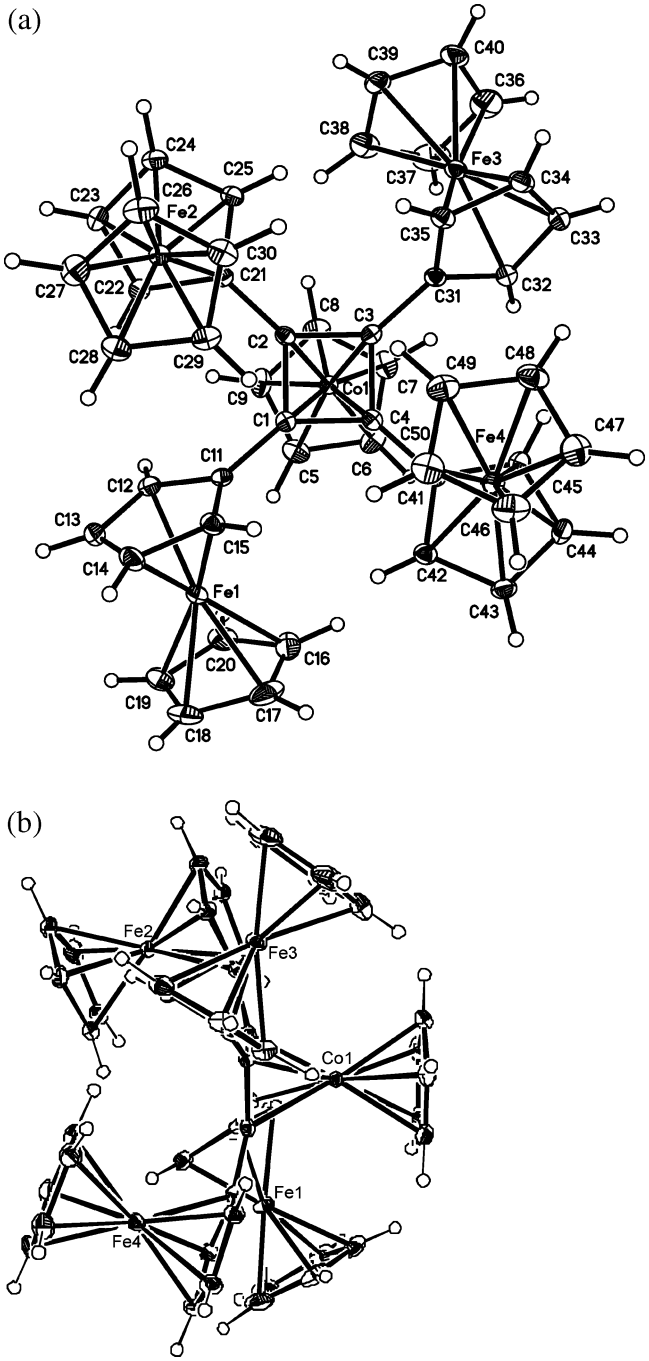

Figure 2. Top view (a) and side view (b) of the molecular structure of $\{(\eta^5\text{-}C_5H_5)Fe(\eta^5\text{-}C_5H_4)\}_4(\eta^4\text{-}C_4)Co(\eta^5\text{-}C_5H_5)$, $\mathbf{1^0}$, with 50% thermal ellipsoids.

the plane defined by the cyclobutadiene ring. However, they are not symmetrically disposed due to the steric bulk of the $Co(\eta^5\text{-}C_5H_5)$ ring (two -0.2 Å and two $+2.1$ Å away from the plane defined by the square ring). The average distance between Fe centers in the distorted square array is 5.86 Å. The ferrocenyl C_5 rings are in nearly eclipsed conformations, and the bond distances of each fragment lie within normal ranges.

The structural solution of $[\mathbf{1^{1+}}][PF_6]$ is less precise due to the presence of 2-fold disorder in one cyclopentadienyl ligand and the $[PF_6]^-$ ion (the asymmetric unit contains half of $\mathbf{1^{1+}}$ and half of the $[PF_6]^-$ ion, and in addition, the $(\eta^5\text{-}C_5H_5)$ unit lies on a mirror plane); however, the basic similarity of the structure to that of $\mathbf{1^0}$ including the relative disposition of the

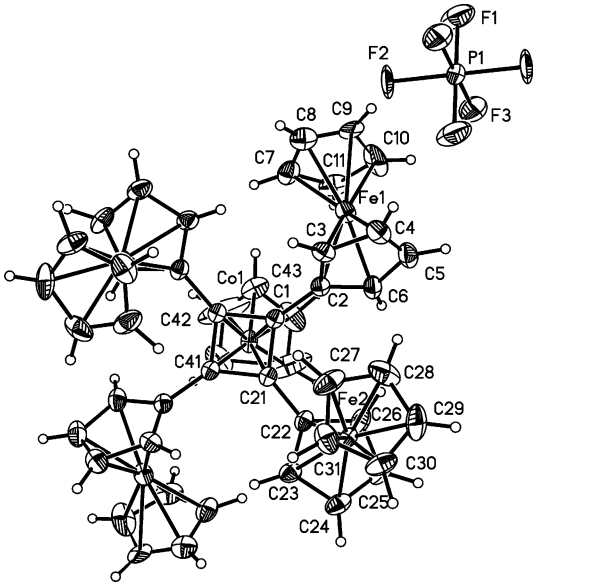

Figure 3. X-ray structure of $[\{(\eta^5\text{-}C_5H_5)Fe(\eta^5\text{-}C_5H_4)\}_4(\eta^4\text{-}C_4)Co(\eta^5\text{-}C_5H_5)][PF_6]$, $\mathbf{1^{1+}}$, with 50% thermal ellipsoids. Only the major components of disorder are shown.

ferrocenyl groups is clear (Figure 3). The average distance between the Fe centers in the cation is 5.94 Å. The crystallographic site symmetry permits only two Fe sites; however, there are three Fe^{II} sites and one Fe^{III} site in each molecule. This leads to disorder and probably accounts for why the U_{iso} values, i.e., the mean-square vibrational amplitudes, of $\mathbf{1^{1+}}$ are about twice as large as for $\mathbf{1^0}$. The latter difference is clearly observed in the Mössbauer spectra (see below).

Vibrational Spectra. Midrange-IR spectroscopy is a proven spectroscopic tool in determining whether a mixed-valence complex is electron delocalized or not on the time scale of molecular vibrations.[30−33] In addition, it has been established that conversion of ferrocene to ferrocenium ion is accompanied by a measurable change in the frequency of the perpendicular C−H bending vibration, i.e., 815 cm^{-1} for ferrocene and 851 cm^{-1} for ferrocenium salts with little change in intensity on oxidation.[30] As a band of $[PF_6]^-$ inconveniently appears at 840 cm^{-1}, the $[BF_4]^-$ salts were used to investigate this region of the spectrum. The FT IR spectra of the tetrafluoroborate salts of $\mathbf{1^0}$, $\mathbf{1^{1+}}$, $\mathbf{1^{2+}}$, and $\mathbf{1^{3+}}$ are shown in Figure 4.

Neutral $\mathbf{1^0}$ shows a single band at 825 cm^{-1} with fine structure, whereas the cations all show two bands ($\mathbf{1^{1+}}$, 825 and 852 cm^{-1}, ~3:1; $\mathbf{1^{2+}}$, 825 and 852 cm^{-1}, ~1:1; $\mathbf{1^{3+}}$, 821 sh and 852 cm^{-1}, ~1:3). These results can be compared with bands observed at 822 and 849 cm^{-1} in mixed-valence 1′,6′-diiodobiferrocenium cation.[33] The observation of two distinct bands in each cation requires all three mixed-valence complexes to have localized Fe^{II} and Fe^{III} ferrocene moieties on the IR time scale; i.e., the electron exchange rate must be $<10^{12}$ s^{-1} at room temperature in the solid state. In addition, the data suggest that $\mathbf{1^{3+}}$ was formed and is substantially pure albeit not analytically

(30) Kramer, J. A.; Hendrickson, D. N. *Inorg. Chem.* **1980**, *19*, 3330−3337.
(31) Dong, T. Y.; Cohn, M. J.; Hendrickson, D. N.; Pierpont, C. G. *J. Am. Chem. Soc.* **1985**, *107*, 4777−4778.
(32) Dong, T. Y.; Schei, C. C.; Hwang, M. Y.; Lee, T. Y.; Yeh, S. K.; Wen, Y. S. *Organometallics* **1992**, *11*, 573−582.
(33) Dong, T. Y.; Kambara, T.; Hendrickson, D. N. *J. Am. Chem. Soc.* **1986**, *108*, 4423−4432.

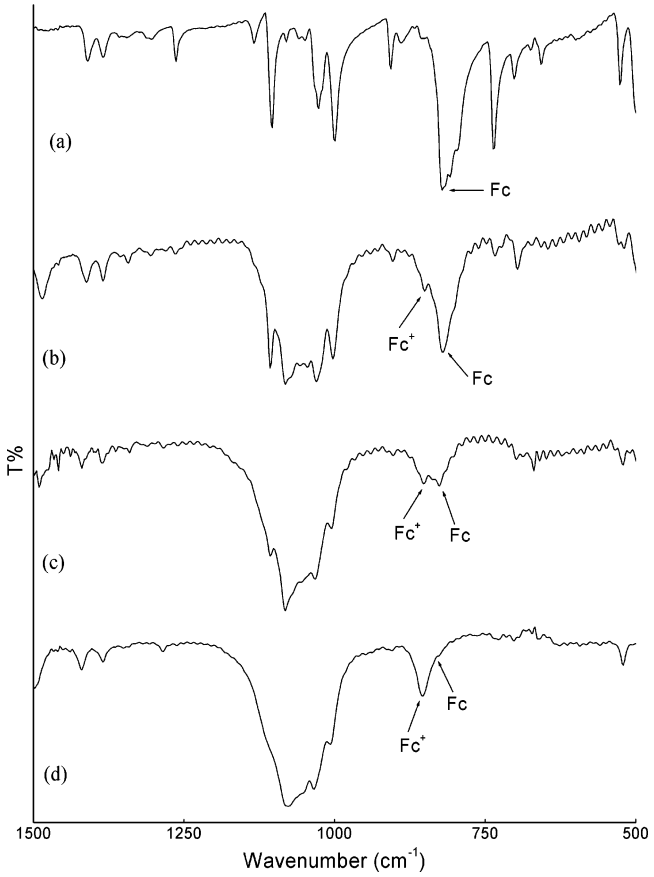

Figure 4. FT-IR spectra in KBr pellets of (a) $\{(\eta^5\text{-}C_5H_5)Fe(\eta^5\text{-}C_5H_4)\}_4(\eta^4\text{-}C_4)Co(\eta^5\text{-}C_5H_5)$, $\mathbf{1^0}$, (b) $[\{(\eta^5\text{-}C_5H_5)Fe(\eta^5\text{-}C_5H_4)\}_4(\eta^4\text{-}C_4)Co(\eta^5\text{-}C_5H_5)][BF_4]$, $\mathbf{1^{1+}}$, (c) $[\{(\eta^5\text{-}C_5H_5)Fe(\eta^5\text{-}C_5H_4)\}_4(\eta^4\text{-}C_4)Co(\eta^5\text{-}C_5H_5)][BF_4]_2$, $\mathbf{1^{2+}}$, and (d) $[\{(\eta^5\text{-}C_5H_5)Fe(\eta^5\text{-}C_5H_4)\}_4(\eta^4\text{-}C_4)Co(\eta^5\text{-}C_5H_5)][BF_4]_3$, $\mathbf{1^{3+}}$, where Fc stands for $(\eta^5\text{-}C_5H_5)Fe(\eta^5\text{-}C_5H_4)$.

pure. This suggests disproportionation of $\mathbf{1^{3+}}$ is not rapid in the solid state but occurs in solution during recrystallization attempts.

Electron Paramagnetic Resonance. The EPR spectra of $\mathbf{1^{1+}}$ and $\mathbf{1^{2+}}$ were examined to look for spin−spin interactions in $\mathbf{1^{2+}}$ that might complicate the QCA application. In addition, this experiment provides g values and permits an independent classification of the electron exchange rate relative to the EPR time scale ($\sim 10^{-9}$ s). The EPR spectra of analytically pure powder samples at 4 K are shown in Figure 5, where it may be observed that the only major difference between the two spectra is that the intensity of the spectrum of $\mathbf{1^{2+}}$ is substantially larger (nearly double) than that of $\mathbf{1^{1+}}$. There is no evidence of spin−spin interaction in $\mathbf{1^{2+}}$ and the associated energy must be small, suggesting essentially independent spins. With an increase in temperature the peaks become broader and less intense although Δg does not change. At 77 K the spectrum of $\mathbf{1^{1+}}$ in a CH_2Cl_2 glass is the same as the powder spectrum albeit broader (Supporting Information). They disappear around 200 K. At the lowest temperature, the spectrum of $\mathbf{1^{1+}}$ yields $g_{\|} = 3.129$, $g_{\perp} = 1.868$, and $\Delta g = 1.261$ and that of $\mathbf{1^{2+}}$ yields $g_{\|} = 3.133$, $g_{\perp} = 1.874$, and $\Delta g = 1.259$. The calculated g factors are 2.362 and 2.369, respectively. The value of Δg has been used previously to classify mixed-valence complexes in terms of the rate of electron transfer between the metal sites on the EPR time scale.[33] For $\Delta g < 0.8$ the rate is considered fast on the EPR time scale; thus, the spectra suggest both $\mathbf{1^{1+}}$ and $\mathbf{1^{2+}}$ are localized on the EPR time scale.

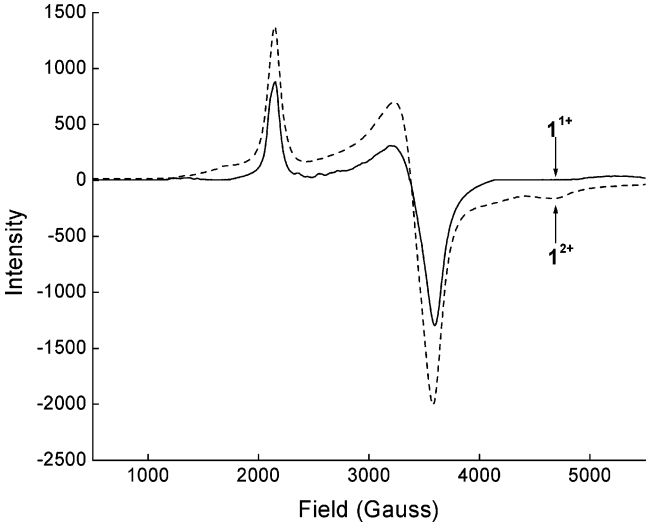

Figure 5. X-band EPR spectra of powdered samples of $[\{(\eta^5\text{-}C_5H_5)Fe(\eta^5\text{-}C_5H_4)\}_4(\eta^4\text{-}C_4)Co(\eta^5\text{-}C_5H_5)][PF_6]$, $\mathbf{1^{1+}}$, and $[(\eta^5\text{-}C_5H_5)Fe(\eta^5\text{-}C_5H_4)\}_4(\eta^4\text{-}C_4)Co(\eta^5\text{-}C_5H_5)][PF_6]_2$, $\mathbf{1^{2+}}$, at 4 K.

Magnetic Susceptibility. The magnetic susceptibilities of $\mathbf{1^{1+}}$ and $\mathbf{1^{2+}}$ have been measured as a function of temperature to corroborate and extend the conclusions drawn from the EPR spectral data. Plots of $1/\chi$ vs T are linear (Figure 6), and the Curie−Weiss parameters were obtained by a fit to $\chi = C/(T - \Theta) + \chi_0$, where Θ is the Curie−Weiss temperature and χ_0 is the temperature-independent contribution to the paramagnetism. The accuracies of the fits for $\mathbf{1^{1+}}$ and $\mathbf{1^{2+}}$ are better than 99.9%. The parameters for $\mathbf{1^{1+}}$ are $C = 0.649$ (emu·K)/mol, $\Theta = -1.25$ K, and $\chi_0 = -2.25 \times 10^{-3}$ emu/mol. The parameters for $\mathbf{1^{2+}}$ are $C = 1.42$ (emu·K)/mol, $\Theta = -2.36$ K, and $\chi_0 = -1.33 \times 10^{-3}$ emu/mol. From these data values of μ_{eff} of 2.27 and 3.36 μ_B are obtained for $\mathbf{1^{1+}}$ and $\mathbf{1^{2+}}$, respectively, values which correspond to one and two unpaired electrons. If there were significant spin−spin interaction in $\mathbf{1^{2+}}$, evidence of either ferro- or antiferromagnetic behavior would be present in the susceptibility curve at low temperatures. As may be seen from Figure 6, $\mathbf{1^{2+}}$ exhibits Curie−Weiss behavior down to 5 K, the lowest temperature measured. Hence, congruent with the EPR spectral measurements, the spin−spin coupling constant is too small to be measured by this technique. Finally, g values can be estimated from these data,[34] giving values of 2.631 for $\mathbf{1^{1+}}$ and 2.383 for $\mathbf{1^{2+}}$, values which are in good agreement with those measured by EPR.

Mössbauer Spectroscopy. To better determine the iron oxidation states and to detect the presence of any electron delocalization in the redox-active complexes, $\mathbf{1^0}$, $\mathbf{1^{1+}}$, and $\mathbf{1^{2+}}$ have been studied by variable-temperature iron-57 Mössbauer spectroscopy. The resulting spectra obtained at 295 and 4.2 K are shown in Figure 7, and some selected hyperfine parameters are given in Table 1. The spectra obtained at intermediate temperatures are very similar to those shown in Figure 7.

As would be expected compound $\mathbf{1^0}$ yields Mössbauer spectra that are very similar to those of ferrocene, a compound which has a large, virtually temperature independent, quadrupole

(34) Cullity, B. D. *Introduction to Magnetic Materials*; Addison-Wesley Publishing Co.: Reading, MA, 1972.

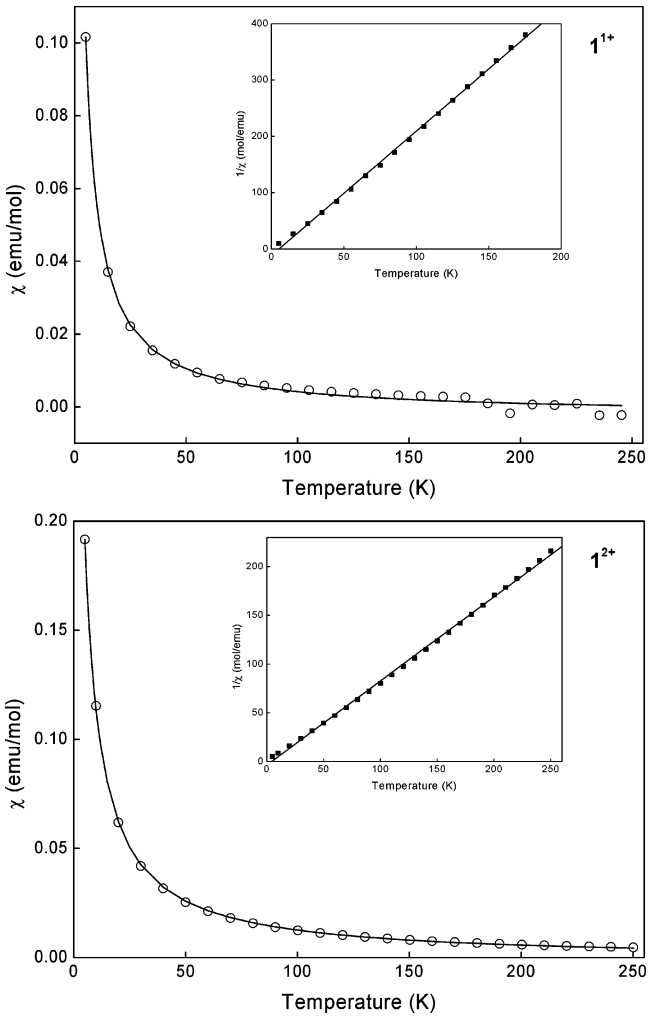

Figure 6. Magnetic susceptibilities (data points) as a function of temperature for (top) [({η^5-C_5H_5)Fe(η^5-C_5H_4)}$_4$(η^4-C_4)Co(η^5-C_5H_5)][PF_6], $\mathbf{1}^{1+}$, and (bottom) [{(η^5-C_5H_5)Fe(η^5-C_5H_4)}$_4$(η^4-C_4)Co(η^5-C_5H_5)][PF_6]$_2$, $\mathbf{1}^{2+}$, with Curie−Weiss fits (solid lines). The insets show plots of $1/\chi$ vs T for each.

splitting of about 2.40 mm/s that is characteristic[35,36] of low-spin Fe^{II} in a highly distorted environment (see the top of Figure 7). Further, $\mathbf{1}^{1+}$ and $\mathbf{1}^{2+}$ also show a quadrupole doublet with this characteristic Fe^{II} doublet, and in all three compounds, the splitting of this doublet, which shows little change with temperature, is slightly smaller than that observed in ferrocene. In addition to this quadrupole doublet, compounds $\mathbf{1}^{1+}$ and $\mathbf{1}^{2+}$ show an additional doublet with a smaller, essentially temperature independent, quadrupole splitting that is characteristic[37−39] of Fe^{III} in the distorted electronic environment of the ferrocenium cation. However, for the Fe^{III} ions the splitting is substantially larger than the splitting of about 0−0.3 mm/s that is often observed[38] for ferrocenium cations.

It should be noted that, although $\mathbf{1}^{0}$ has four crystallographically distinct iron sites, the Fe^{II} ions at these four sites are so chemically similar that they are not resolved in the Mössbauer spectra of $\mathbf{1}^{0}$. Indeed, the line widths observed for $\mathbf{1}^{0}$ at 295 and 4.2 K are almost the same as those of the α-iron calibration line width of ca. 0.24−0.26 mm/s. In contrast, $\mathbf{1}^{1+}$ has only two crystallographically distinct iron sites and a molecule of $\mathbf{1}^{1+}$ contains two Fe1 and two Fe2 crystallographic sites, but only one of these four iron sites is oxidized to Fe^{III}, an oxidation that introduces disorder into the molecule. Despite this disorder, the Fe^{II} line widths in $\mathbf{1}^{1+}$ are small and very similar to the Fe^{II} line widths in $\mathbf{1}^{0}$. Further, even the Fe^{III} line width in $\mathbf{1}^{1+}$ is not especially large, indicating that, on a microscopic scale, the molecule must adjust its local bonding to the nature of the iron oxidation state.

In agreement with the infrared spectral results presented above, in neither $\mathbf{1}^{1+}$ nor $\mathbf{1}^{2+}$ between 4.2 and 295 K is there any indication of any electron delocalization between the Fe^{II} and Fe^{III} ions, and on the Mössbauer time scale of ca. 10^{-7} s, both compounds behave as Robin and Day class II localized discrete valence compounds. In contrast, it should be noted that a mixed-valence biferrocene compound with an electron exchange rate greater than 10^{7} s^{-1} shows a single averaged quadrupole doublet with a splitting of 1.0−1.1 mm/s.[30,32,33]

The temperature dependence of the isomer shifts in $\mathbf{1}^{0}$, $\mathbf{1}^{1+}$, and $\mathbf{1}^{2+}$ is shown in Figure 8. Once again the observed isomer shifts, and their temperature dependence, are characteristic[36,38,39] of Fe^{II} or Fe^{III} in a ferrocene- or ferrocenium-like environment. The temperature dependence of the isomer shift has been fit with the Debye model for the second-order Doppler shift, and the resulting fits are shown by the solid lines in Figure 8. In these fits the effective vibrating mass has been held constant at 57 g/mol as would be expected for the iron-57 nuclide. The resulting effective Mössbauer temperatures are rather high at 450(30) to 600(30) K, values which are consistent with the strong bonding found in the ferrocene and the ferrocenium ion.

Because the recoil-free fractions are quite different for Fe^{II} in ferrocene and Fe^{III} in a ferrocenium ion,[39] the area ratio for the Fe^{II} to Fe^{III} doublets in $\mathbf{1}^{1+}$ and $\mathbf{1}^{2+}$ vary substantially at higher temperatures from the expected 3:1 and 1:1 ratios, respectively; see Table 1. However, at lower temperatures, as the recoil-free fractions approach unity, the area ratios approach but do not reach the expected values. To better understand why these ratios are not closer to the expected values, we have measured the full temperature dependence of the Mössbauer spectra of $\mathbf{1}^{0}$, $\mathbf{1}^{1+}$, and $\mathbf{1}^{2+}$ between 4.2 and 295 K. The resulting temperature dependence of the spectral absorption areas are given in units of [(% ϵ)(mm/s)]/(mg of Fe^{II}/cm^2) or [(% ϵ)-(mm/s)]/(mg of Fe^{III}/cm^2) in Table 1, and the temperature dependence of the logarithm of the area is shown in Figure 9. Once again, this temperature dependence has been fit with the Debye model for the vibrations of a solid, and the fits, which assume a mass of 57 g/mol for the iron-57 nuclide, are shown as solid lines in Figure 9.

As would be expected the temperature variations for the Fe^{II} ions in $\mathbf{1}^{0}$, $\mathbf{1}^{1+}$, and $\mathbf{1}^{2+}$ are very similar and yield effective Mössbauer temperatures of 146(6), 132(2), and 139(4) K, respectively. Further, as would be expected for the stronger bonding of the ferrocenium Fe^{III} ion, their spectral absorption areas are larger than for Fe^{II}, see Figure 9, and the Fe^{III} ions in $\mathbf{1}^{1+}$ and $\mathbf{1}^{2+}$ have similar effective Mössbauer temperatures of 150(2) and 152(2) K, respectively, values that are somewhat larger than for the Fe^{II} ions.

(35) Herber, R. H.; Nowik, I. *Solid State Sci.* **2002**, *4*, 691−694.
(36) Wright, M. E.; Long, G. J.; Tharp, D. E.; Nelson, G. O. *Organometallics* **1986**, *5*, 779−784.
(37) Morrison, W. H.; Hendrickson, D. N. *Inorg. Chem.* **1975**, *14*, 2331−2346.
(38) Deschenaux, R.; Schweissguth, M.; Vilches, M. T.; Levelut, A. M.; Hautot, D.; Long, G. J.; Luneau, D. *Organometallics* **1999**, *18*, 5553−5559.
(39) Parish, R. V. In *The Organic Chemistry of Iron*; Koerner von Gustorf, E. A., Grevels, F., Fischler, I., Eds.; Academic Press: New York, 1978; Vol. 1, p 192.

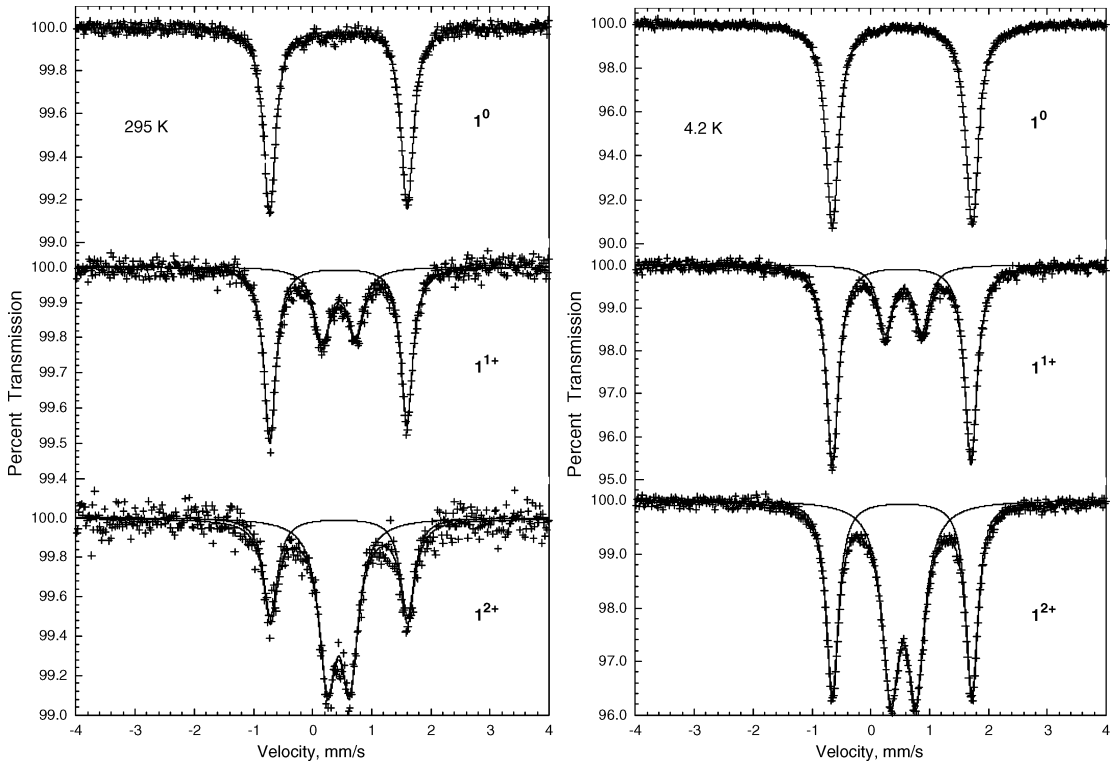

Figure 7. Mössbauer spectra of $\{(\eta^5\text{-}C_5H_5)Fe(\eta^5\text{-}C_5H_4)\}_4(\eta^4\text{-}C_4)Co(\eta^5\text{-}C_5H_5)$, $\mathbf{1^0}$, $[\{(\eta^5\text{-}C_5H_5)Fe(\eta^5\text{-}C_5H_4)\}_4(\eta^4\text{-}C_4)Co(\eta^5\text{-}C_5H_5)][BF_4]$, $\mathbf{1^{1+}}$, and $[\{(\eta^5\text{-}C_5H_5)Fe(\eta^5\text{-}C_5H_4)\}_4(\eta^4\text{-}C_4)Co(\eta^5\text{-}C_5H_5)][BF_4]_2$, $\mathbf{1^{2+}}$, obtained at 295 K, left, and 4.2 K, right.

Table 1. Selected Mössbauer Spectral Hyperfine Parameters

comp	*T*, K	δ,[a] mm/s	ΔE_Q, mm/s	Γ, mm/s	area, %	area, [(% ϵ)(mm/s)]/ (mg of Fe/cm^2)	assignment
$\mathbf{1^0}$	295	0.438	2.33	0.25	100	0.45	Fe^{II}
	95	0.527	2.35	0.31	100	1.80	Fe^{II}
	4.2	0.536	2.37	0.27	100	2.70	Fe^{II}
$\mathbf{1^{1+}}[PF_6]$	295	0.440	2.32	0.24	63.9	0.25	Fe^{II}
		0.447	0.56	0.32	36.1	0.47	Fe^{III}
	95	0.525	2.34	0.28	72.2	1.18	Fe^{II}
		0.545	0.60	0.31	27.8	1.52	Fe^{III}
	4.2	0.538	2.36	0.25	71.3	1.92	Fe^{II}
		0.563	0.62	0.30	28.7	2.19	Fe^{III}
$\mathbf{1^{2+}}[PF_6]_2$	295	0.448	2.31	0.29	36.0	0.46	Fe^{II}
		0.439	0.38	0.34	64.0	0.81	Fe^{III}
	95	0.525	2.36	0.26	40.2	1.77	Fe^{II}
		0.535	0.42	0.35	59.8	2.61	Fe^{III}
	4.2	0.534	2.37	0.25	43.1	2.88	Fe^{II}
		0.549	0.44	0.35	56.9	3.77	Fe^{III}
Cp_2Fe[b]	295	0.447	2.40	0.23	100		Fe^{II}
	85	0.533	2.40	0.26	100		Fe^{II}

[a] The isomer shifts are given relative to the value for room temperature α-iron foil. [b] Data obtained from ref 36.

The second-order Doppler shift of the Mössbauer spectral isomer shift is directly related[40] to the mean square velocity of the iron nuclide, a velocity that depends on the frequency distribution of the normal vibrating modes of the solid. In contrast, the temperature dependence of the recoil-free fraction is directly related to the mean square amplitude of vibration of the iron nucleus, an amplitude that depends differently on the frequency distribution of the normal vibrating modes of the solid. Hence, the temperature dependencies of the isomer shift and of the recoil-free fraction do not probe the same phonon modes in the lattice, and as is the case herein, differing Mössbauer lattice temperatures may be extracted from these measurements.

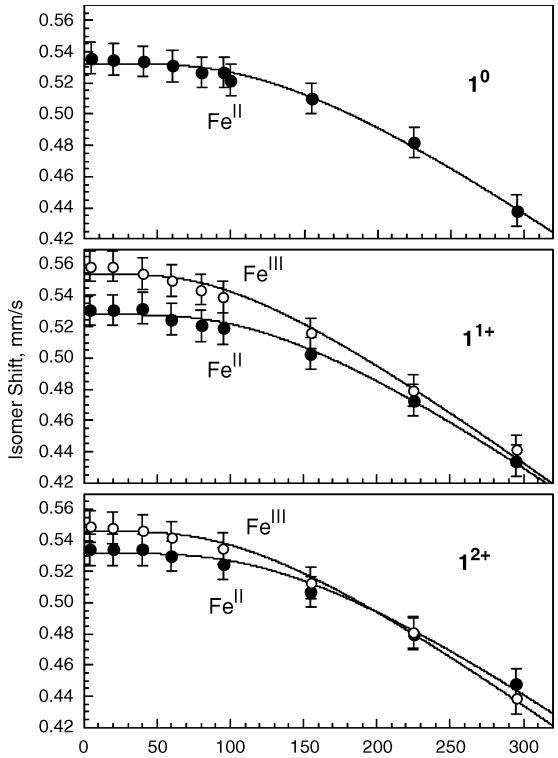

Figure 8. Temperature dependence of the isomer shifts observed for $\{(\eta^5\text{-}C_5H_5)Fe(\eta^5\text{-}C_5H_4)\}_4(\eta^4\text{-}C_4)Co(\eta^5\text{-}C_5H_5)$, $\mathbf{1^0}$, $[\{(\eta^5\text{-}C_5H_5)Fe(\eta^5\text{-}C_5H_4)\}_4(\eta^4\text{-}C_4)Co(\eta^5\text{-}C_5H_5)][BF_4]$, $\mathbf{1^{1+}}$, and $\{(\eta^5\text{-}C_5H_5)Fe(\eta^5\text{-}C_5H_4)\}_4(\eta^4\text{-}C_4)Co(\eta^5\text{-}C_5H_5)][BF_4]_2$, $\mathbf{1^{2+}}$. The solid lines correspond to fits with a Debye model for the second-order Doppler shift as discussed in the text.

(40) Herber, R. H. In *Chemical Mössbauer Spectroscopy*; Herber, R. H., Ed.; Plenum Press: New York, 1984; p 199.

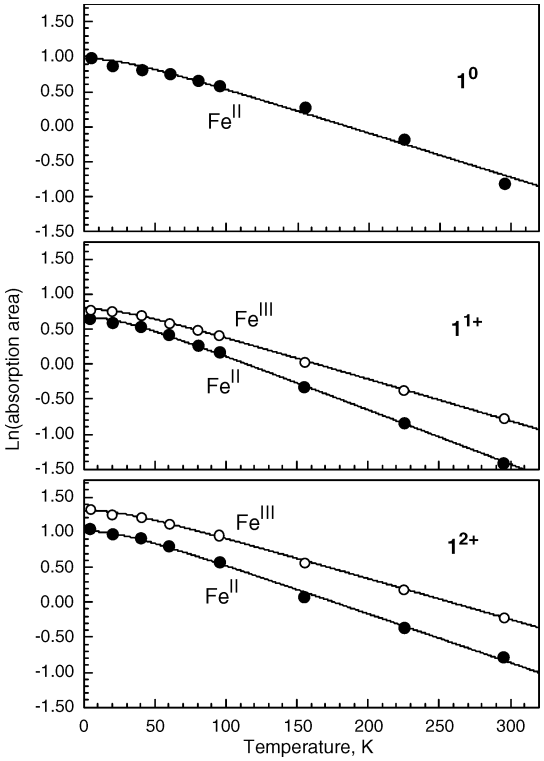

Figure 9. Temperature dependence of the logarithm of the Mössbauer spectral absorption area, expressed in [(% ϵ)(mm/s)]/[(mg of Fe)/cm^2], observed for {(η^5-C_5H_5)Fe(η^5-C_5H_4)}$_4$(η^4-C$_4$)Co(η^5-C_5H_5), **1^0**, [{(η^5-C_5H_5)-Fe(η^5-C_5H_4)}$_4$(η^4-C$_4$)Co(η^5-C_5H_5)][BF$_4$], **1^{1+}**, and [{(η^5-C_5H_5)Fe(η^5-C_5H_4)}$_4$-(η^4-C$_4$)Co(η^5-C_5H_5)][BF$_4$]$_2$, **1^{2+}**. The solid lines correspond to fits with the Debye model for the vibrations of a solid as discussed in the text. The error bars are approximately the size of the data points.

Because the spectra of all three of the compounds have been measured under very similar geometric and γ-ray-counting conditions, it is possible to compare the absolute spectral absorption areas for the three compounds. As may be noted in Figure 9 and Table 1, the weighted average spectral absorption areas for both the Fe^{II} and Fe^{III} ions in **1^{1+}** are significantly smaller than in **1^0** and **1^{2+}**. At 95 K the values are 1.80, 1.27, and 2.27 [(% ϵ)(mm/s)]/(mg of Fe/cm^2) for **1^0**, **1^{1+}**, and **1^{2+}**, respectively, whereas at 4.2 K the values are 2.70, 2.00, and 3.39 [(% ϵ)(mm/s)]/(mg of Fe/cm^2). This reduction in spectral absorption areas and the associated reduction in the recoil-free fraction in **1^{1+}** relative to **1^0** is a consequence of the very different thermal factors for the iron sites in the two compounds. In **1^0** the isotropic thermal parameter, U_{iso}, averaged for the four Fe sites, corresponds to a root mean square vibrational amplitude of 0.0131 Å, a very typical value for a ferrocene-like molecule. In contrast, in **1^{1+}**, U_{iso}, averaged for the two Fe sites, corresponds to a mean square vibrational amplitude of 0.0256 Å, i.e., a value twice that of **1^0** and atypically large even for a ferrocenium-like ion. The difference in U_{iso}, which likely results from the disorder of Fe^{III} over the four iron sites in a molecule of **1^{1+}**, is clearly reflected in the reduced Mössbauer spectral absorption areas observed for **1^{1+}**; see Figure 9. This reduction is a clear indication that in **1^{1+}** only one out of the four Fe^{II} sites in **1^0** has been oxidized to Fe^{III}. The alternative possibility that in one-quarter of the molecules of **1^{1+}** all four of the Fe^{II} sites have been oxidized to Fe^{III} is eliminated.

Even though the U_{iso} values, i.e., the mean square vibrational amplitudes, are different in **1^0** and **1^{1+}** and lead to different recoil-free fractions, the temperature dependence of the mean square vibrational amplitudes of the iron nuclide is similar in all three compounds and leads to similar Mössbauer lattice temperatures as is indicated above.

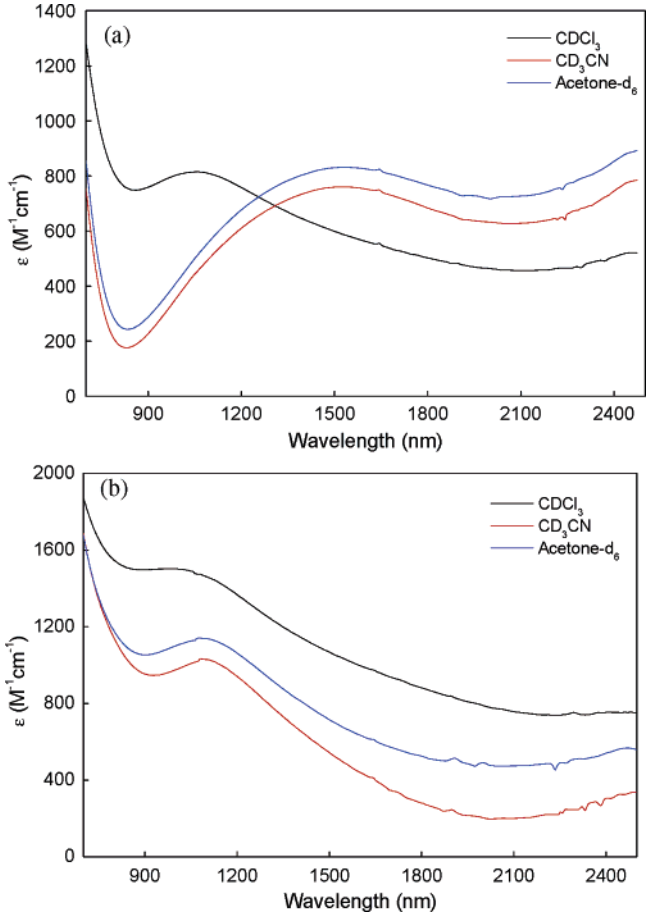

Figure 10. Near-IR spectra of (a) [{(η^5-C_5H_5)Fe(η^5-C_5H_4)}$_4$(η^4-C$_4$)Co-(η^5-C_5H_5)][PF$_6$], **1^{1+}**, and (b) [{(η^5-C_5H_5)Fe(η^5-C_5H_4)}$_4$(η^4-C$_4$)Co(η^5-C_5H_5)]-[PF$_6$]$_2$, **1^2**, in $CDCl_3$, CD_3CN, and $CD_3C(O)CD_3$.

Near-IR Spectroscopy. One characteristic of Robin and Day class II and III mixed-valence complexes is the presence of absorption bands in the near-infrared energy range corresponding to transitions from the ground state to intervalence charge transfer states, i.e., transitions in which an electron is moved from one metal center to the other. Hence, we sought evidence confirming intervalence charge transfer states in **1^{1+}** and **1^{2+}**. Analysis of these bands and the effects of solvent on the band characteristics with Hush theory[41] provides parameters that report on, e.g., ground-state delocalization. This permits a comparison of these new mixed-valence complexes with known dinuclear mixed-valence complexes. For reference, the UV−vis and near-IR spectra of **1^0** (Figure 1, Supporting Information) show no bands in the near-IR region.

Figure 10 shows the near-IR spectra of **1^{1+}** and **1^{2+}** in three different deuterated solvents; deuterated solvents were used to reduce interference from the C−H overtone bands.[42] The standard numerical parameters derived from these spectra are gathered in Table 1 in the Supporting Information. The bands observed for **1^{1+}** and **1^{2+}** are assigned to intervalence charge transfer bands corresponding to transfer of an electron between

(41) Hush, N. S. *Prog. Inorg. Chem.* **1967**, *8*, 391−444.
(42) Powers, M. J.; Meyer, T. J. *J. Am. Chem. Soc.* **1978**, *100*, 4393−4398.

ferrocene and ferrocenium centers. Those of $\mathbf{1}^{2+}$ occur at higher energy than those of $\mathbf{1}^{1+}$ in a given solvent. In addition, the near-IR spectrum of impure $\mathbf{1}^{3+}$ in acetone-d_6 shows one broad band at 922 nm. The higher energy of the band relative to that for $\mathbf{1}^{2+}$ is consistent with it being due to an intervalence charge transfer transition in $\mathbf{1}^{3+}$. On standing, the near-IR band maximum of $\mathbf{1}^{3+}$ shifts to lower energy with time, suggesting disproportionation into $\mathbf{1}^{2+}$ and $\mathbf{1}^{4+}$ as expected on the basis of the small comproportionation constant derived from the electrochemical results. These observations corroborate evidence for the formation of $\mathbf{1}^{3+}$ from the midrange-IR results presented above. Finally, as expected, impure $\mathbf{1}^{4+}$, prepared as described above, shows no absorption in the near-IR region.

Beyond these qualitative conclusions, the solvent dependence of the band maxima and the Hush parameters calculated from the band energies, bandwidths, and intensities add further detail. By using the energies of the band maxima and the differences in the redox potentials as a measure of the internal energy differences between oxidation states, the calculated bandwidths at half-maximum intensity can be compared with those measured. As shown in Table 1 (Supporting Information) these average 1.3 and 1.1 for $\mathbf{1}^{1+}$ and $\mathbf{1}^{2+}$, respectively. For Robin and Day class II complexes values of 1.1−1.4 have been reported.[42−44] An alternative parameter to compare is the so-called delocalization parameter, α^2, which is a function of the extinction coefficient, bandwidth, and band energy. Once again the average delocalization parameters calculated for $\mathbf{1}^{1+}$ and $\mathbf{1}^{2+}$ (Table 1, Supporting Information) are similar to those reported for class II systems.[42,45,46] Finally, the solvent dependence of the band energy has been used to classify mixed-valence complexes. Both $\mathbf{1}^{1+}$ and $\mathbf{1}^{2+}$ show Franck−Condon inner sphere optical activation energies (extrapolated band energies at zero solvent polarity from a linear plot of band energy vs solvent polarity shown in Figure 2, Supporting Information) that are larger than those reported for class III compounds[47,48] but in line with those of class II compounds.[42] Finally, the greater dependence on solvent polarity for $\mathbf{1}^{1+}$ as opposed to $\mathbf{1}^{2+}$ suggests the latter may lie in the more recently defined class II−III category with delocalized solvent but a localized electron.[49]

The midrange-IR, EPR, and Mössbauer spectral studies have placed an upper limit on the electron exchange rate of 10^7 s^{-1} in the solid state. In reference to the proposed QCA application, an upper limit is not particularly helpful as very slow switching rates are not useful. Some measure of the actual rate is necessary to evaluate $\mathbf{1}^{2+}$. The near-IR spectra permit an estimate of a thermally activated rate in solution from Hush theory.[41] Assuming the Hush approach applies, the electron transfer rate $k_{et} = \kappa\nu_n \exp(-\nu_{max}/4kT)$. From $\kappa\nu_n$ (transmission factor times vibrational frequency) $= 1 \times 6 \times 10^{12}$ s^{-1} and ν_{max} (band energy) $= 9.3 \times 10^3$ cm^{-1} for $\mathbf{1}^{2+}$ in acetone, the solution electron transfer rate is about 10^8 s^{-1} at room temperature in the absence of an electric field. Presumably it would be higher in a nonzero field. The thermal free energy barrier implied by the Hush treatment corresponds to 2.3×10^3 cm^{-1} or 6.6 kcal/mol.

Paramagnetic Nuclear Magnetic Resonance. The structural and spectroscopic data gathered above define the nuclear geometries and significant aspects of the electronic structures of $\mathbf{1}^{1+}$ and $\mathbf{1}^{2+}$ but do not answer two crucial questions. The electron transfer rate estimated in the previous section posits a small thermal barrier for reaction. Can variable-temperature paramagnetic NMR spectra provide support for this hypothesis? Given the class II or II−III behavior of $\mathbf{1}^{1+}$ and $\mathbf{1}^{2+}$, what is the disposition of the holes and/or electrons in $\mathbf{1}^{2+}$? Do the holes and/or electrons have the trans disposition that is required both for QCA and for the minimization of the Coulombic repulsion? Again paramagnetic NMR experiments have the potential to distinguish between the two different symmetries. In fact, there must be a significant energy preference for the trans arrangement to use the molecule for QCA. In QCA theory the difference in energy between the cis and trans arrangements of the holes and/or electrons is known as the "kink" energy. If this energy is too small relative to the thermal energy at the temperature of operation, the binary signal transmitted through the cells will become garbled.

Before looking at the paramagnetic NMR data, it is necessary to examine the variable-temperature ^{1}H NMR spectra of $\mathbf{1}^{0}$ because its simple room-temperature spectrum reflects an apparent symmetry higher than that observed in the solid state. Any fluxional behavior must be documented in $\mathbf{1}^{0}$ because similar barriers to structural reorganization will be present in $\mathbf{1}^{1+}$ and $\mathbf{1}^{2+}$ as well. The spectra from room temperature to 193 K are shown in Figure 11, and a labeled structure of $\mathbf{1}^{0}$ is shown in Scheme 2. Additional detail is shown in expanded spectra in Figures 5 and 6 in the Supporting Information. Four signals are observed for the ferrocene moieties at room temperature corresponding to effective 4-fold symmetry on the NMR time scale. The triplet at 4.82 ppm, which is assigned to the eight H_α protons, is a convenient descriptor of the descent in symmetry as the temperature decreases. This resonance broadens and then splits into two equal peaks at 4.5 and 5.1 ppm at 233 K (Figure 6, Supporting Information). Each of these resonances splits into two area-equivalent peaks at 4.35 and 4.52 ppm and 4.86 and 5.46 ppm at the lowest temperature. The resonance corresponding to the cyclopentadienyl protons of the Co ligand remains a relatively sharp singlet at all temperatures. The barrier associated with the higher temperature coalescence, estimated from the frequency difference of the two signals at 233 K, is 4.9 kcal/mol. When one considers the approximations involved, this value is close to the 6.6 kcal/mol estimated for the electron exchange process from the near-IR data.

A simple interpretation of the variable-temperature ^{1}H NMR of $\mathbf{1}^{0}$ follows. At room temperature, the ferrocenyl groups freely rotate around the connecting C−C bonds and all eight H_α protons are equivalent. At 233 K, complete rotation ceases and the ferrocene 1, 3 and ferrocene 2, 4 pairs lie on opposite sides of the cyclobutadiene ring (Scheme 2). However, a rocking motion continues, making $H_{\alpha1}$ equivalent to $H_{\alpha2}$ on each ferrocene moiety. Finally, at the lowest temperature, $H_{\alpha1}$ and $H_{\alpha2}$ become inequivalent as the rocking motion is frozen out and the two sets of four protons split into four sets of two

(43) Powers, M. J.; Meyer, T. J. *Inorg. Chem.* **1978**, *17*, 2955−2958.
(44) Colbran, S. B.; Robinson, B. H.; Simpson, J. *Organometallics* **1983**, *2*, 952−957.
(45) Dowling, N.; Henry, P. M.; Lewis, N. A.; Taube, H. *Inorg. Chem.* **1981**, *20*, 2345−2348.
(46) Li, Z. H.; Beatty, A. M.; Fehlner, T. P. *Inorg. Chem.* **2003**, *42*, 5707−5714.
(47) Chellamma, S.; Lieberman, M. *Inorg. Chem.* **2001**, *40*, 3177−3180.
(48) Creutz, C. *Inorg. Chem.* **1978**, *17*, 3723−3725.
(49) Demadis, K. D.; Hartshorn, C. M.; Meyer, T. J. *Chem. Rev.* **2001**, *101*, 2655−2685.

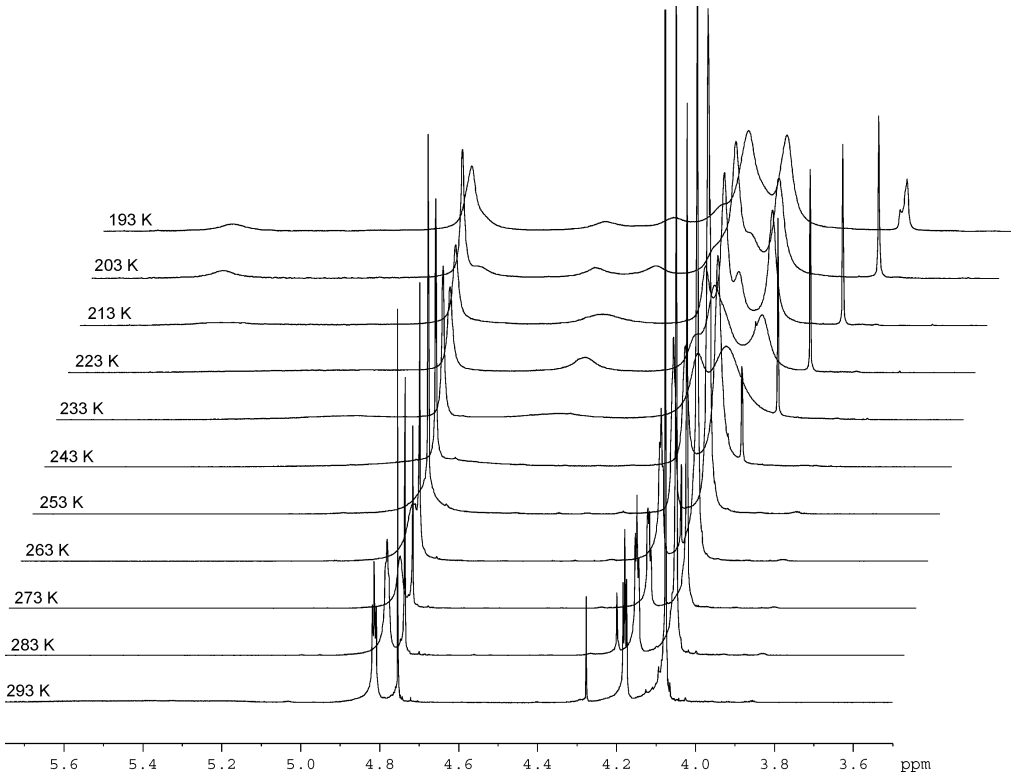

Figure 11. ^{1}H variable-temperature NMR spectra of $\{(\eta^5\text{-}C_5H_5)Fe(\eta^5\text{-}C_5H_4)\}_4(\eta^4\text{-}C_4)Co(\eta^5\text{-}C_5H_5)$, $\mathbf{1^0}$, in toluene-d_8 at 400 MHz. The resonance at 4.28 in the 293 K spectrum is due to the solvent of crystallization (CH_2Cl_2).

Scheme 2. Schematic Drawing of Hindered Rotation around the Connecting C−C Bonds To Explain the Variable-Temperature ^{1}H NMR of $\mathbf{1^0}$

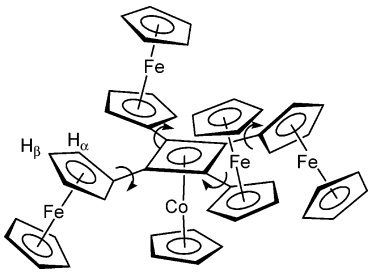

protons. However, it is not the details of the mechanism that are of greatest importance here but rather the fact that at the lowest temperature the spectrum is consistent with the solid-state structure.

The paramagnetic NMR spectra of $\mathbf{1^{1+}}$ and $\mathbf{1^{2+}}$ are expected to exhibit broad lines and less predictable positions due to large paramagnetic shifts, thereby making the problem of assignment very difficult. As the hindered rotation of the ferrocenyl groups in $\mathbf{1^0}$ is due mainly to steric interactions, the rotation of the ferrocenyl groups in the paramagnetic cations will have barriers similar to those of $\mathbf{1^0}$. Coalescence temperatures, however, may differ as large paramagnetic shifts will change the pertinent resonance frequencies. The third complicating factor, and the one of principal interest here, is the rate of electron exchange between ferrocene and ferrocenium centers. The analysis of the near-IR data suggests electron transfer which is rapid on the NMR time scale at room temperature. The same near-IR data suggest a thermal barrier for electron exchange large enough to make the electron transfer rate slow on the NMR time scale at low temperature. That being the case, we expect that the change in the spectra in going from the fast to slow exchange regimes (delocalized to localized) will produce dramatic changes in the appearance of the NMR spectra. That is, under conditions of slow electron transfer between the iron centers, the broad, highly shifted ferrocenium resonances should be easily distinguishable from the less shifted, sharper ferrocene resonances. The spectra of $\mathbf{1^{1+}}$ and $\mathbf{1^{2+}}$ provide two independent sources of information.

The variable-temperature NMR spectra of analytically pure $\mathbf{1^{1+}}$ and $\mathbf{1^{2+}}$ are shown in Figures 12 and 13. They are clearly those of paramagnetic species as the shifts of four broad resonances in each depend linearly on $1/T$ in accord with the expected Curie law behavior (Tables 2 and 3 and Figures 3 and 4, Supporting Information). Consider $\mathbf{1^{1+}}$ first and for reference note that ferrocenium tetrafluroborate in acetone shows a broad resonance at 31 ppm whereas ferrocene exhibits a sharp resonance at 4 ppm. The three major signals at room temperature were the same at two concentrations differing by a factor of 4 and can be reasonably assigned to the η^5-C_5H_5 rings of the central Co (3.1 ppm) and the averaged ferrocene/ferrocenium moieties (8.0 and 11.0 ppm). For rapid electron exhange on the NMR time scale, an average of one ferrocenium ion and three ferrocenes would give a single, weight-averaged resonance at 11 ppm, thereby justifying this assignment.

At 248 K, three broad peaks with large parmagnetic shifts can be assigned to a ferrocenium moiety (24.4, H_α; 11.4, η^5-C_5H_5; −5.9, H_β) whereas two peaks in the ratio of 2:1 (6.6, −0.1 ppm) are assigned to the ferrocenyl groups trans and cis to the ferrocenium group. A sharp resonance at 3.2 ppm is assigned to the Co η^5-C_5H_5 ligand protons. Hence, the electron transfer rate is slower than 10^3 s^{-1} at 248 K, which implies a barrier greater than 2.4 kcal/mol. At lower temperatures the Co η^5-C_5H_5 resonance splits (2.8 and 3.8 ppm at 203 K as shown

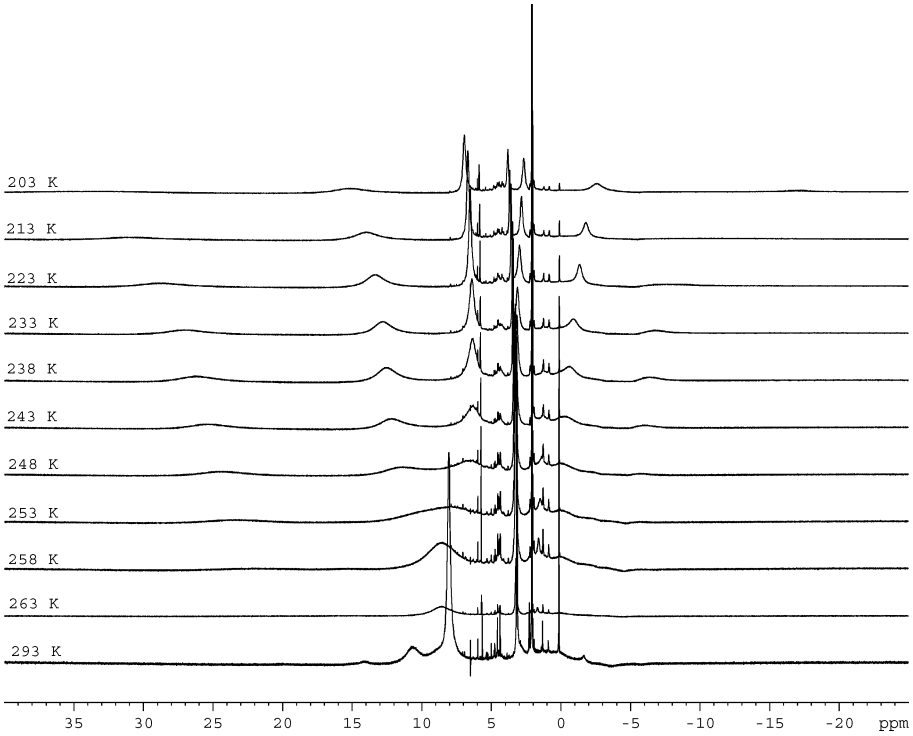

Figure 12. ^{1}H variable-temperature NMR spectra of about 2 mM $[\{(\eta^5\text{-}C_5H_5)Fe(\eta^5\text{-}C_5H_4)\}_4(\eta^4\text{-}C_4)Co(\eta^5\text{-}C_5H_5)][PF_6]$, $\mathbf{1}^{1+}$, in acetone-d_6 at 400 MHz.

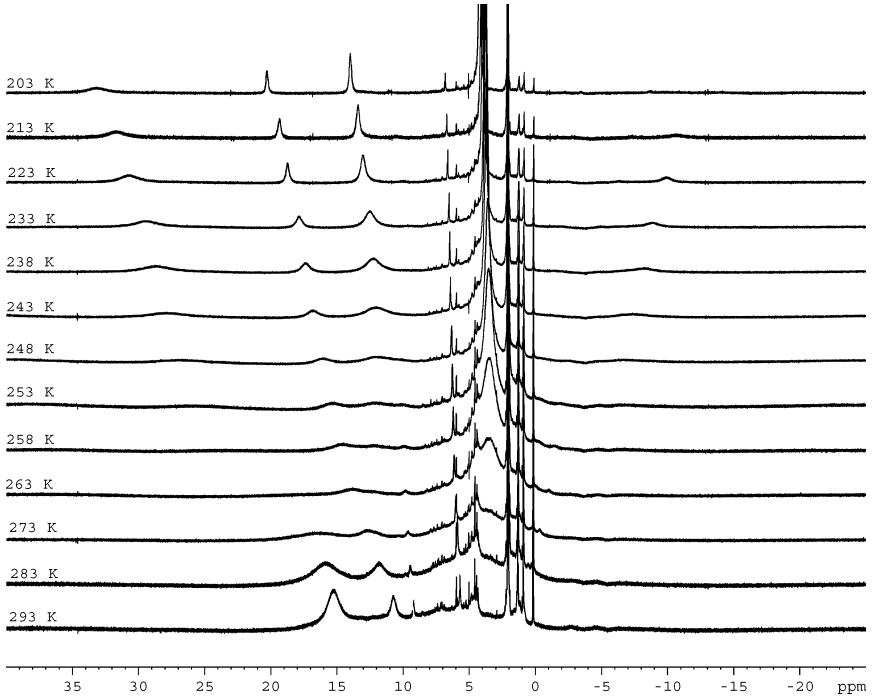

Figure 13. ^{1}H variable-temperature NMR spectra of about 1.5 mM $[\{(\eta^5\text{-}C_5H_5)Fe(\eta^5\text{-}C_5H_4)\}_4(\eta^4\text{-}C_4)Co(\eta^5\text{-}C_5H_5)][CF_3SO_3]_2$, $\mathbf{1}^{2+}$, in acetone-d_6 at 400 MHz.

in Figure 7 in the Supporting Information) as expected if the ferrocenium group can be either above or below the cyclobutadiene ligand plane (Scheme 2).

Even though we are unable to make detailed assignments, the qualitative changes in the spectra with temperature support the presence of a thermal barrier for electron exchange. This would corroborate the Hush analysis of the near-IR data with one caveat. It is known that in a mixed-valence biferrocene cation the coplanar and noncoplanar arrangements of the ferrocenes yield very different electron transfer rates.[26] This means the barrier to free rotation around the connecting C−C bonds in $\mathbf{1}^{1+}$ may actually constitute the thermal barrier to electron exchange in these mixed-valence complexes; i.e., in the solid-state structure the π systems of the central linker and those of the ferrocenes are not aligned, and thus, the electron exchange is slow.

The presence of a thermal barrier to electron transfer is also evident in the paramagnetic NMR spectrum of $\mathbf{1}^{2+}$. At 293 K

there are three peaks not due to impurities: a peak at 9.2 ppm assigned to the Co η^5-C_5H_5 ligand and peaks at 10.7 and 15.2 ppm assigned to averaged ferrocene/ferrocenium. That is, rapid electron transfer on the NMR time scale between one ferrocenium ion and one ferrocene would give a weight-averaged signal at 17 ppm. For proof of the presence of a thermal barrier, a key observation is the appearance of a broad resonance at 3.4 ppm at 263 K and lower temperatures (Figure 8, Supporting Information). This resonance is assigned to the two ferrocenyl groups on freezing out of the electron exchange and, as a consequence, suggests the presence of a thermal barrier in accord with the analysis of the spectrum of $\mathbf{1}^{1+}$.

When free rotation of the ferrocenyl groups around the connecting C−C bonds can no longer occur, a species with adjacent 1,2-paramagnetic centers will have a single isomer whereas one with 1,3-paramagnetic centers will have two (one with two ferrocenes located cis to the Co fragment and one with two ferrocenes located trans; see Scheme 2). The key is the resonance of the Co η^5-C_5H_5 ligand because for 1,2-paramagnetic centers there should only be one resonance whereas for the 1,3-paramagnetic centers there will be two. Unfortunately, the 9.2 ppm room temperature resonance assigned to the Co η^5-C_5H_5 ligand broadens and disappears on cooling, and no unambiguous assignment at lower temperatures was possible. Although this is more consistent with 1,3-paramagnetic centers, the data do not provide a definitive answer to the question of the preferred arrangement of the oxidized and unoxidized ferrocenyl groups.

Conclusions

The crystallographic data on $\mathbf{1}^{0}$ and $\mathbf{1}^{1+}$ and spectroscopic data on $\mathbf{1}^{0}$, $\mathbf{1}^{1+}$, and $\mathbf{1}^{2+}$ show that $\mathbf{1}^{2+}$ possesses properties that permit its use as a molecular QCA building block. The complete picture suggests that the valence trapping observed in the spectroscopic experiments in the solid state originates from the misalignment of the conjugated systems of the molecular "dots" and the square central linker. This has important consequences for the use of this molecule for QCA. For efficient electronic coupling and electron exchange, all four unsubstituted ferrocenyl η^5-C_5H_5 ligands will have to be linked to a surface. This would force all the ferrocenyl moieties to be trans to the Co(η^5-C_5H_5) group and align the π systems of the η^5-C_5H_4R and η^4-C_4R_4 groups for efficient switching between the two degenerate arrangements of charge found in $\mathbf{1}^{2+}$. It would also remove the distortions of the four Fe centers from a square array as found in the structures of $\mathbf{1}^{0}$ and $\mathbf{1}^{1+}$ as well as serve to anchor and align the square on the chosen substrate. We conclude that $\mathbf{1}^{2+}$ is an excellent candidate for a molecular QCA cell.

Experimental Section

All reactions were carried out using standard Schlenk techniques.[50] Solvents were distilled immediately before use under N_2 from the following dry agents: sodium benzophenone ketyl for hexane and diethyl ether, molten sodium metal for toluene, and calcium hydride for CH_2Cl_2. Other solvents were spectroscopic grade and dried over activated 3 Å molecular sieves before use. Reagents from Aldrich, Acros, or Strem were used as purchased.

The following instrumentation and conditions were used: IR, Perkin-Elmer Paragon 1000 FT-IR as KBr pellets; UV−vis; Beckman DU-7500; near-IR, Thermo Nicolet Nexus 670 FT-IR; mass spectra (FAB^+), JEPL JMS-AX505HA from *p*-nitrobenzyl alcohol; NMR, Varian Unity Plus (300 MHz) and Bruker DPX Avance (400 MHz), ^1H ($CDCl_3$, 7.27 ppm) and ^{13}C ($CDCl_3$, 77.23 ppm); EPR, Bruker EMX X-band, Oxford continuous-flow cryostat (ESR 900), room temperature to 4 K, powder samples, 77 K CH_2Cl_2 glass; electrochemistry, BAS Epsilon-EC with Pt working, Pt-flag counter, and Pt-wire pseudoreference electrodes with tetrabutylammonium hexafluorophosphate supporting electrolyte in a drybox, $E_{1/2}$(ferrocene couple) = 0.344 V; ^{57}Fe Mössbauer spectra, constant-acceleration spectrometer with a room-temperature rhodium matrix cobalt-57 source, calibrated at room temperature with α-iron foil, relative accuracy of the isomer shifts ±0.005 mm/s, relative accuracy of the quadrupole splittings and line widths ±0.01 mm/s, relative accuracy of the areas ±0.4%, absolute accuracy about twice these values; magnetic susceptibility, Quantum Design SQUID magnetometer, 10 mg sample size, 5−250 K, at 3 T field strength; elemental analysis, M-H-W Laboratories.

{(η^5-C_5H_5)Fe(η^5-C_5H_4)}$_4$(η^4-C_4)Co(η^5-C_5H_5), $\mathbf{1}^{0}$. The procedure used was a modification of that used by Rausch et al.[27] To a solution of (η^5-C_5H_5)Fe(η^5-C_5H_4)C≡C(η^5-C_5H_4)Fe(η^5-C_5H_5) (418 mg, 1.06 mmol) in xylenes (25 mL) was added 95.5 mg (0.53 mmol) of CpCo-$(CO)_2$. The solution was refluxed with stirring for 24 h and then allowed to cool to room temperature. The solvent was removed in vacuo, and the resulting orange-brown solid was extracted with toluene, filtered through Celite, and chromatographed on a neutral alumina column. Elution with toluene afforded 300 mg (62%) of brown-orange solid $\mathbf{1}^{0}$. Brown-orange block crystals were obtained from recrystallization from CH_2Cl_2/hexane. Anal. Calcd for $C_{49}H_{41}Fe_4Co$: C, 64.52; H, 4.53. Found: C, 64.64; H, 4.65. ^1H NMR ($CDCl_3$): δ 4.82 (t, J = 2 Hz, 8H, α-H), 4.79 (s, 5H, Cp−Co), 4.32 (t, J = 2 Hz, 8H, β-H), 4.11 (s, 20H, Cp−Fe). ^{13}C NMR ($CDCl_3$): δ 82.9 (4C, cyclobutadiene), 81.3 (5C, Cp−Co), 70.2 (8C, β-C), 69.9 (4C, α-C), 69.6 (20C, Cp−Fe), 67.8 (8*C*, γ-C). FAB-MS: *m*/*z* 912 (M^+).

[{(η^5-C_5H_5)Fe(η^5-C_5H_4)}$_4$(η^4-C_4)Co(η^5-C_5H_5)][PF_6], $\mathbf{1}^{1+}$. To a solution of 45.6 mg (0.05 mmol) of $\mathbf{1}^{0}$ in 15 mL of CH_2Cl_2 was added [η^5-C_5H_5)$_2$Fe][PF_6] (16.6 mg, 0.05 mmol). The color changed to deep brown in 5 min. The reaction mixture was stirred for about 3 h, and the solvent was removed under vacuum. The resulting brown solid was washed with ether three times and dried under vacuum to give 40 mg of a dark brown solid. The yield was 76%. Dark brown crystals suitable for X-ray analysis were obtained by crystallization from CH_2Cl_2/hexane. Anal. Calcd for $C_{49}H_{41}CoF_6Fe_4P$: C, 55.76; H, 3.91. Found: C, 55.72; H, 3.83. FT-IR (KBr): 850 cm^{-1} (δ_{C-H} for [η^5-C_5H_5)$_2$Fe]$^+$), 833 cm^{-1} (ν_{PF_6}), 821 (δ_{C-H} for η^5-C_5H_5)$_2$Fe). FAB-MS: *m*/*z* 911.9 (M − PF_6). The tetrafluoroborate salt was synthesized by a similar procedure.

[{(η^5-C_5H_5)Fe(η^5-C_5H_4)C(O)CH_3][PF_6]. This oxidizing agent was prepared with a modified literature procedure.[29] To 154 mg (0.675 mmol) of (η^5-C_5H_5)Fe(η^5-C_5H_4)C(O)CH_3 in ethyl ether was added $AgPF_6$ (170 mg, 0.67 mmol), which resulted in an immediate color change to blue and the formation of a blue precipitate. The reaction mixture was stirred for about 30 min, dried under vacuum, extracted with CH_2Cl_2, and filtered through Celite. The filtrate was concentrated to 5 mL, and 50 mL of ether was added slowly with stirring to generate a blue precipitate. The precipitate was washed with ether three times and dried under vacuum to give 120 mg (48%).

[{(η^5-C_5H_5)Fe(η^5-C_5H_4)}$_4$(η^4-C_4)Co(η^5-C_5H_5)][PF_6]$_2$, $\mathbf{1}^{2+}$. To a stirred solution of $\mathbf{1}^{0}$ (45.6 mg, 0.05 mmol) in CH_2Cl_2 (15 mL) was added 37.3 mg (0.1 mmol) of [(η^5-C_5H_5)Fe(η^5-C_5H_4)C(O)CH_3]PF_6, which resulted in an immediate color change from orange to deep red-brown. After 2 h, the solution was evaporated to dryness. The resulting red-brown residue was washed with diethyl ether three times and dried under vacuum to give 57 mg (95%) of a red-brown powder. Anal. Calcd for $C_{49}H_{41}CoF_{12}Fe_4P_2$: C, 48.96; H, 3.44. Found: C, 48.76; H, 3.60. The tetrafluoroborate and triflate salts were synthesized in a similar fashion.

(50) Shriver, D. F.; Drezdzon, M. A. *The Manipulation of Air-sensitive Compounds*, 2nd ed.; Wiley: New York, 1986.

[{(η^5-C_5H_5)Fe(η^5-C_5H_4)}$_4$(η^4-C_4)Co(η^5-C_5H_5)][BF_4]$_3$, 1^{3+}. A 30 mg (0.09 mmol) sample of [(η^5-C_5H_5)Fe(η^5-C_5H_4)C(O)CH_3]BF_4 was added to the solution of $\mathbf{1^0}$ (14 mg, 0.015 mmol) in 10 mL of CH_2Cl_2. A red-brown solid was precipitated immediately. The reaction mixture was stirred for about 2 h. The red-brown solid was filtered off, washed with CH_2Cl_2 and ether twice, and dried under vacuum. FT-IR (KBr): 853 cm^{-1} (δ_{C-H} for Fc^+), 821 (δ_{C-H} for Fc). Due to its instability, neither analysis nor further purification was possible.

Single-Crystal X-ray Structure Determinations. Single crystals of $\mathbf{1^0}$ and $\mathbf{1^{1+}}$ suitable for X-ray diffraction were obtained by slow diffusion from CH_2Cl_2 to hexane. Crystalline samples were placed in an inert oil, mounted on a glass pin, and transferred to the cold gas stream of the diffractometer. Crystal data were collected and integrated using a Bruker Apex system, with graphite-monochromated Mo Kα (λ = 0.71073 Å) radiation at 100 K. The structures were solved by heavy atom methods using SHELXS-97 and refined using SHELXL-97 (Sheldrick, G. M., University of Göttingen). Non-hydrogen atoms were found by successive full-matrix least-squares refinement on F^2 and refined with anisotropic thermal parameters. In $\mathbf{1^0}$ all hydrogen atoms were located from difference Fourier maps and allowed to refine isotropically with fixed thermal parameters [u_{ij} = 1.2U_{ij}(eq) for the atom to which they are bonded]. In $\mathbf{1^{1+}}$ all hydrogen atoms were placed at idealized positions, and a riding model was applied, with fixed thermal parameters as with $\mathbf{1^0}$.

Acknowledgment. We thank Professor R. Hayes and Dr. J. Velasco for aid with the EPR measurements and Dr. F. Gascoin for his aid with the susceptibility measurements. We acknowledge with thanks the financial support of ONR/DARPA (Grant N00014-00-1-0746), NSF (Grant CCF04-03760), the Fonds National de la Recherche Scientifique, Belgium (Grant 9.456595), and the Ministère de la Région Wallonne (Grant RW/115012).

Supporting Information Available: Ten pages of tables and figures mentioned in the text and CIF files for the structures of $\mathbf{1^0}$ and $\mathbf{1^{1+}}$. This material is available free of charge via the Internet at http://pubs.acs.org.

JA0550935